# Cellulose carbon fiber: plasma synthesis and characterization

Andrii Zaitsev, Sandy Moisan, Fabienne Poncin-Epaillard

# Cellulose carbon fiber: plasma synthesis and characterization

*Andrii Zaitsev[1,2], Sandy Moisan[1], Fabienne Poncin-Epaillard[2*]*

[1]IRT Jules Verne, Chemin du Chaffault, 44340 Bouguenais, France
[2]Institut des Molécules et Matériaux du Mans (IMMM), UMR CNRS 6283, Le Mans Université, Avenue Olivier Messiaen, 72085 Le Mans Cedex, France

* Corresponding author: Fabienne.Poncin-Epaillard@univ-lemans.fr, ORCID ID: 0000-0001-5254-1203

**Acknowledgments**

This work is part of the French FORCE project, supervised by the IRT Jules Verne (Bouguenais, France) and CANOE research center (Bordeaux, France).

**Abstract**

Carbon fibers widely used in automotive, aerospace and energy present the advantage over conventional materials of combining low weight and high strength. This advantage is counterbalanced by their significant cost and the release of toxic substances during carbonization. Bio-sourced cellulose materials-like and eco-friendlier plasma carbonization technologies will help to overcome these challenges. The dependence of the carbonization yield on the plasma parameters (pressure, power, duration...) is illustrated showing that it is a fast process leading to an efficient carbon fiber well characterized for the chemical, morphological and mechanical aspects. Indeed, the plasma-carbonization of stretched cellulose fibers containing various CNT proportions (0 %, 0.01 %, 0.1 %, 0.3%, 0.6%) gives rise to an important residue close to the theoretical value (44.5%). The synthesized and surface-functionalized homogeneous, non-porous carbon fibers present a high ratio of Raman D/G bands reflected a high yield of the carbon organization and, therefore, inducing good mechanical properties. The plasma-carbonization mechanism essentially involves the ejection of hydroxyl groups from cellulose and their subsequent dissociation in plasma.

**Key-words:** cellulose; carbon fiber; chemical properties; fiber conversion processes.

## 1. Introduction

The development of carbon fibers (CF) is hindered by its cost and therefore, it is restricted for areas where its price plays a secondary role in the choice of materials (mainly the aerospace industry and high-level sport). The carbonization precursor (polyacrylonitrile, PAN) is about 55 % of the final price due to the high cost of its monomer. In order to reduce the CF price and to stimulate their emergence towards a wider range of markets, alternative precursors issued from renewable sources such as cellulose are still looking for, even if the first CF were historically based on cellulose materials (Schalamon 1973). Indeed, cellulose is a crystalline and thermosensitive natural product promoting the formation of an ordered structure during the carbonization step. Its carbonization yield is less efficient than the PAN one, respectively 10 - 15 % and 60 %, since some by-products are issued from the cellulose depolymerization rather than its carbonization (Tang 1964). Tang *et al.* (1964) showed that the thermal degradation and depolymerization are initiated in the same temperature range 240 - 400 °C. Even if the major chemical reactions are completed at 400 °C, carbonization continues until 900 - 1500 °C. In

this temperature range, non-carbon atoms are expelled, the fiber is then composed of at least 95 % carbon. Densification and contraction of the observed fibers are explained by the appearance of aromatic and polycyclic structures. Finally, the carbonization ends with the formation of graphite-like structure formed by $sp^3$ and $sp^2$ carbons ( Konhin 1985; Tang 1964).

Another carbonization process similar to that used for the PAN-based fibers (Byrne 2016) occurs in an inert atmosphere (dinitrogen, argon) in order to avoid the degradation of the fiber. The temperature rises up to 1000 - 1500 °C. The heating rate plays an important role. If the temperature rise is too fast, the fiber will have structural defects, i.e. porosity, due to rapid evaporation of small molecules and its mechanical performance will be altered. In an opposite manner, a too long procedure, even if yielding high performance fibers, becomes tedious and unacceptable. Moreover, the final mechanical properties cannot be compared to those of ex-PAN fibers (tensile strength = 0.5 - 1.5 GPa, Young's modulus = 25 - 100 GPa compared to typically 3 GPa and 250 GPa respectively for ex-PAN) (Frank 2012), but the ex-cellulose CF has exceptionally low thermal conductivity (3 W / (m.K) compared to 20 W / (m.K) for ex-PAN) and lower density (1.4 g / $cm^3$ compared to 1.7 g / $cm^3$ for ex-PAN) (Delhaes 2013). Several reviews summarize all assets and drawbacks of processes and characterizations of the different carbon fibers (Dumanh 2012; Goodhew 1975).

In order to study a less energy-consuming process, plasma technologies could be applied. However, in our knowledge, the state of the art deals only with the PAN carbonization (Kim 2015; Paulauskas 2002). Indeed, PAN was Ar plasma-treated in a microwave chamber at high discharge powers (100 - 1000 W) during 4 min (Kim 2015). The plasma-carbonized ex-PAN presents similar mechanical properties (resistance of 1.4 GPa, Young's modulus of 120 GPa) without any surface defects (porosities). Its mechanical properties may be increased by a two-step plasma process (Paulauskas 2002). The overall advantage of such technology is short duration (15 - 30 min).

This paper deals here with the plasma-carbonization of cellulose fibers at different proportions of carbon nanotubes (CNT) added for a higher final properties' improvement. It describes also the mechanism study of such a process versus various plasma parameters influencing reactive species densities interacting on fiber surface and the characterization of the final ex-cellulose CF. Such a plasma-treatment will also act as the stabilization step.

## 2. Experimental part

### *2.1 Microwave plasma chamber*

A plasma reactor with distributed microwave sources (Boréal Plasmas 7050) was used. Twelve microwave sources (electronic cyclotronic resonance (ECR) applicators) are distributed along the circumference (Fig. 1). This configuration allows working at low pressure (*p*, down to 0.1 Pa) leading to a high plasma homogeneity.

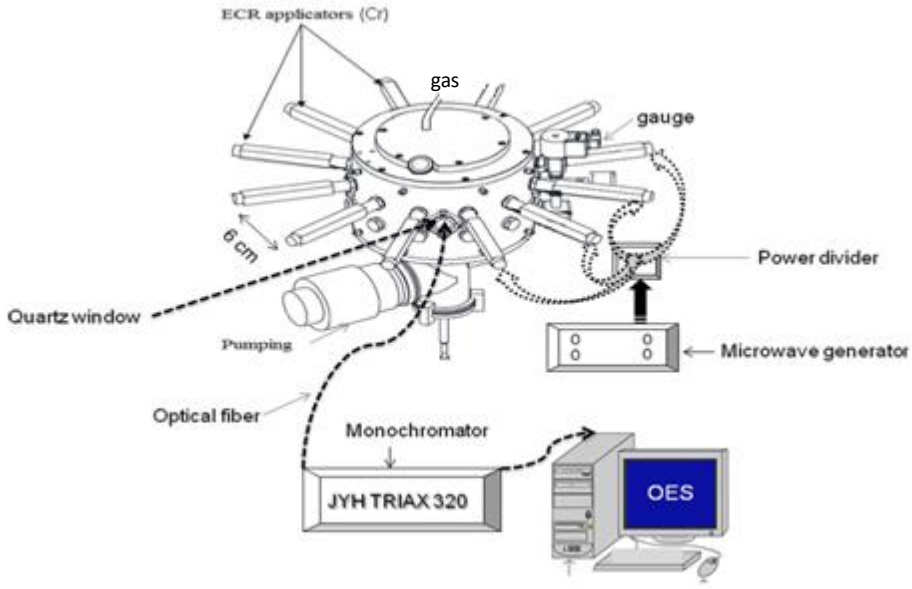


Fig. 1 Scheme of the microwave plasma reactor used for the plasma-carbonization

The system was pumped to a base pressure of $5\times10^{-2}$ Pa using a turbomolecular pump (Adixen ATH300Ci) backed up by a dry pump (Adixen ACP28G). The pressure in the chamber was measured using a Pirani-cold cathode combined gauge (Pfeiffer PKR251). Ar, $N_2$ gases (AirLiquide, 99 %) were introduced through the upper flange of the plasma chamber. The flow rates (*Q*) were comprised between 1 and 40 sccm (measured by Brooks mass flow meters). The pressure (*p*) dependent of flow rate was comprised between 0.1 Pa and 8 Pa (measured by capacitive gauge Pfeiffer CCR364). The cellulose fiber was fixed on the sample holder located in different positions on the microwave applicator or strained between two applicators. The plasma was generated using a microwave generator (Sairem GMP20KED 2.45 GHz) and the reflected power was minimized separately for every applicator. The applicators located in the vicinity of working one (or two, depending on the sample holder configuration) were not powered (microwave radiation was absorbed and dissipated by external radiators). This allows for minimizing their influence on the plasma parameters. The carbonization time (*t*) and the power input (*P*) were varied between 1 and 30 min, 16 W and 160 W (/ applicator). These power values are respectively minimum to initiate carbonization process and maximum permitted by microwave generator. The parameters domains are chosen in order to maintain a stable plasma phase avoiding the fibers burning. Pulsed mode of plasma

was achieved by pulsed generator HP 33120A ($10^{-3}$ - $10^{7}$ Hz), connected to the power input of microwave generator. Each treatment was at least repeated 5 times.

The plasma temperature was determined by optical emission spectroscopy (OES). The plasma radiation was collected through a quartz window located at the upper flange of the chamber and transmitted through an optical fiber to JobinYvon Horiba TRIAX 320 scanning monochromator (grating 1200 grooves / mm blazed at 500 nm, focal length of 320 mm, f/4.1 in aperture ratio, high spectral resolution of 0.06 nm in the first order for diffraction, dispersion of 2.64 nm / mm). The monochromator, that scans a wavelength range from 180 nm up to 1000 nm, was connected to a JY Symphony CCD camera-array (1024 x 256 pixels). For each experimental condition, a total of 10 spectra were averaged over an integration time of 10 ms, with a background correction performed by subtracting the baseline. This approach allowed deducing accurate intensity values of atomic lines and molecular bands of excited fragments. It should be noted that the statistical error of emission intensity measurements is about 10 %. For the calculation of plasma temperature, excitation temperature of $Ar^{I}$ system was determined to use equation (1):

$$\ln\left(\frac{\varepsilon*\lambda}{g*A}\right) = C - \frac{E_K}{kT} \quad (1)$$

where ε - coefficient of emission, λ - wavelength of emission, g - transition probability, A - Einstein coefficient, $E_K$ - higher level energy, k - Boltzmann constant, T - temperature, C – arbitrary constant. The temperature value was deduced from the slope of the plot $\ln\left(\frac{\varepsilon*\lambda}{g*A}\right) = f(\frac{E}{k})$.

*2.2 Materials*

The cellulose fibers were supplied by CANOE. The cellulose fibers with different proportions of carbon nanotubes (CNT, 0 %, 0.01 %, 0.1 %, 0.3%, 0.6%) were spun by CANOE from cellulose fluff (*Pinus pinaster*, Tembec, France) and each fiber (diameter ≈ 28 µm, density ≈ 1.92 g.cm$^{-3}$, sample length ≈ 12 cm) is composed of 1000 strands. These fibers will be referred as CANOE fibers. The second type, rayon fibers, is industrially available and will be referred as model fibers.

*2.3. Analyses*

*2.3.1 Determination of the residue of plasma-carbonization (R)*

The residue ($R$) is calculated from the ratio between the fiber weight before ($m_0$, taking into account the content of CNT) and after treatment (m, taking into account the content of CNT) (2).

$$R = \frac{m}{m_0} x100\ (\%)\ (2)$$

*2.3.2 Raman spectroscopy*

Raman analyzes on cellulose fibers were conducted on the Horiba Xplora spectrometer with a confocal Olympus BX41 microscope and equipped with a 532 nm green laser and an objective (x 100). The acquisitions (2 scans, 40 s / scan) were run on the wavenumber area 500 - 2000 $cm^{-1}$ with a laser power ≈ 5 mW. The dispersive system consists of a network with 1800 strokes / mm. The spectra were taken on at least 3 different fibers, within 2 measurements per fiber.

*2.3.3 FTIR spectroscopy*

FTIR spectra in MIR wavenumber range (4000 - 600 $cm^{-1}$) were recorded using a Bruker VERTEX70v spectrometer in ATR mode. Spectra were collected at a resolution of 4 $cm^{-1}$ over 32 scans including the subtraction of $CO_2$ / $H_2O$ bands.

*2.3.4 XPS spectroscopy*

XPS has been carried out with a PHI Quantera SXM spectrometer using a monochromatic Al $K_\alpha$ X-ray source (1486.6 eV), with magnetic confinement charge neutralization. The hybrid lens magnification mode was used with the slot aperture resulting in an analyzed area of 700 x 300 µm². Charge stabilization was achieved. Spectra were recorded with a step size of 0.5 eV and a pass energy of 80 eV. Spectra were calibrated using the $C_{1s}$ peak at 284.8 eV. For semi-quantification of carbon, high resolution spectra were recorded with a step size of 0.1 eV and a pass energy of 20 eV. Emission angle of photoelectrons was 90°. Spectra decomposition was performed using Casa XPS software.

*2.3.5 Scanning electron microscopy (SEM)*

SEM-micrographs (Scanning Electron Microscopy) were taken by the microscope JEOL-JSM-6510LV operating at 5 - 20 kV with tungsten filament. Beforehand, the fibers were sputter-deposited with a thin layer (~20 nm) of gold.

*2.3.6 Mechanic tests*

Mechanical tests of fibers were carried out on LRX 2k5 tensile testing machine (Lloyd Instruments, Ametek, USA) according to single cellulose fiber tensile test (ISO 11566). Fiber length was 10 mm and gauge full scale 10 N, test speed 1 mm / min. Pull test was conducted on series of 10 samples, mean fiber diameter was calculated from 10 measurements by scanning electron microscopy.

## 3. Results

*3.1. Influence of the plasma homogeneity on the plasma-carbonization of cellulose fibers*

In order to carbonize the cellulose fibers, the ECR excitation was selected since it produces a higher plasma density compared to other plasma excitations. However, such a plasma induces a gradient of plasma density from its source to the center of the chamber. Indeed, the plasma is particularly dense near the microwave applicator to the extent of a few cm (radially towards the applicator). Beyond this area, a plasma diffusion regime is established in the overall chamber volume. This diffusive plasma is characterized by a lower density. Several tests with different plasma parameters sets avoiding the fiber burning ($Q_{N2}$ = 5 - 40 sccm, $p$ =1 - 8 Pa, $t$ = 5 - 30 min, $P$ = 80 - 160 W) were therefore necessary in order to reach optimal positioning of the fibers for their carbonization. Finally, two different positions were selected. The first one consists of wrap the fibers on alumina sample-holder which surrounds the powered applicator (Fig. 2a). Such a configuration enables the homogeneous carbonization. With the second position (Fig. 2b), more applicable for industrial purpose, the fiber located between the two powered applicators is completely surrounded by the plasma phase and for preserving its shape it can be strained by 100 g load during its treatment. Both positions were studied with an Ar plasma chosen rather than the dinitrogen plasma in order to enhance the bombardment by heavy particles, neutrals, ions or metastables.

(a) (b)

Fig. 2 Sample-holders used for cellulose fibers plasma-carbonization

*3.2. Influence of the fiber nature (structure and chemical formulation) on the plasma-carbonization yield*

Different CANOE fibers containing various proportions of CNT**s** were Ar plasma-treated for carbonization. The obtained results on residue appearance (R) were compared with CANOE fiber**s** without CNT**s** and a model sample based on Rayon material (Fig. 3). The horizontal line corresponds to the theoretical and stoichiometric yield of cellulose carbonization (44.5 %). Whatever the fiber, the proportion of residue material is time-dependent with a fast decrease for short duration; then a plateau, whose value is strongly related to the fiber chemical composition**,** appears for longer times. The lowest residue proportion (5 %) is obtained with the model fiber and must be interpreted as degradation, depolymerization mechani**s**ms with the appearance of volatile products rather than carbonization. The residue yield of cellulose fiber is dependent on the CNT proportion. Higher the latter is, closer to the theoretical value the former is. However, increasing the CNT concentration beyond 0.3% does no longer affect the plateau value, probably due to a too high electronic conductivity avoiding any charge and heating effect. In comparison, typical yields for conventional thermal process are fewer than 30 % ( Akato 2012; Kim 2016).

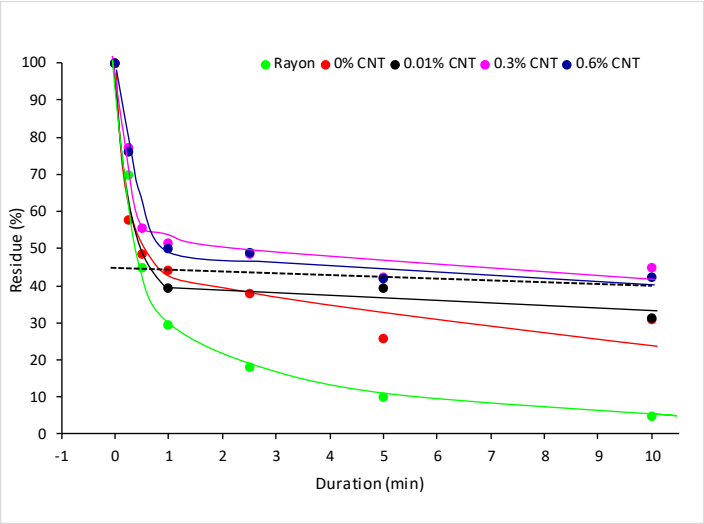


Fig. 3 Dependence of the residue yield on plasma duration and chemical nature of the fiber ($Q_{Ar}$ = 40 sccm, $P$ = 160 W, sample-holder = Fig. 2a, dashed line = theoretical carbonization yield)

The elaboration of carbon structures is related to the depolymerization of cellulose with the appearance of volatile products of low molecular weight (Ramiah 1970; Yang 2007) and the kinetic control. The incorporated additives containing phosphorus, sulfur or nitrogen atoms (called as impurities in Table 3) partially inhibit this depolymerization in favor of the creation of carbon structures (Pappa 1995; Price 1997). Since the CANOE fibers contain traces of sulfur and phosphorus due to the spinning process, this could explain the difference in behavior observed between two types of fibers (CANOE and model). Moreover, the presence of CNT plays an additional beneficial role explained by the contribution of better electrical and thermal conductivity facilitating the evacuation of the charged (electronic or ionic) particles, of the heat during the plasma treatment and thus, limiting the depolymerization. An additional effect of CNT could also be due to the enhancement of the crystalline carbon domain creation since CNTs are also known as crystallization nuclei (Broza 2005; McNally 2005; Ryan 2007). In respect of such results, the plasma behavior will be further studied only with 0.3% CNT CANOE fibers.

*3.3. Influence of the plasma parameters on the plasma-carbonization yield of 0.3 % CNT CANOE fibers*

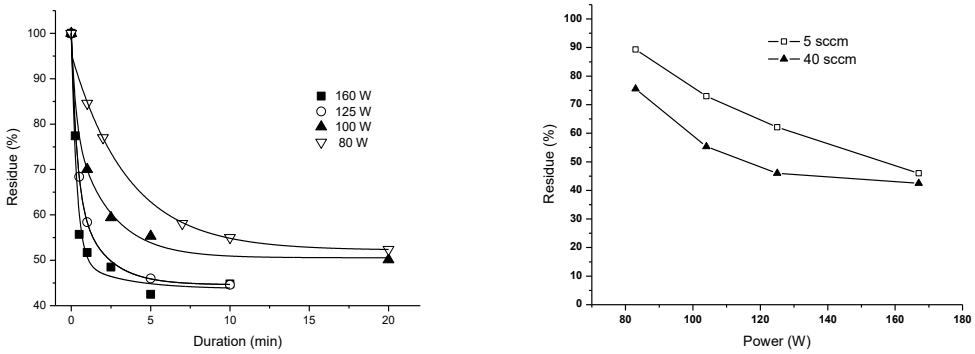


(a) (b)

Fig. 4 Dependence of the residue yield of 0.3% CNT CANOE fibers on Ar plasma parameters (a): on power -$Q_{Ar}$ = 40 sccm, (b): on Ar flow, $t$ = 5 min, $P$ = 160 W (sample-holder = Fig. 2a)

The power parameter is related to the number of electrons injected into the plasma chamber and thus defines the density of the plasma phase. This influences the carbonization yield. Indeed, at the minimum discharge power (80 W), the plateau is reached after 20 min of treatment (Fig. 4a). It should be noted that this plateau is above stoichiometric yield (53 % against 44.5 %). This means that carbonization is not complete or can only be reached over very long periods of time. At 100 W, the kinetics is much faster, the plateau is obtained in 10 min. The stoichiometric residue is still not reached. Only injected powers greater than or equal to 125 W enables it for

obtaining carbonization with 44.5 % of the residue after 10 min. Finally, at maximum power (160 W), the plateau is reached a little faster (5 min).

The working pressure and the linked Ar flow rate have an opposite effect on the density of the ions and on their mean free path in the plasma phase. When one increases, the other decreases with pressure. To study the influence of these two physical quantities on carbonization, tests with two extreme values of flow (5 and 40 sccm) were conducted (Fig. 4b). This figure shows that the carbonization rate is flow-dependent; increasing with this parameter but according to a law in function of the flow value: rise quasi-linear for 5 sccm and non-linear for 40 sccm. However, it is interesting to note that the points at 160 W of the two curves are superimposed. The important conclusion to be drawn is that the 44.5 % carbon residue is obtained at lower powers when the argon flow is high (120 W at 40 sccm against 160 W at 5 sccm). One may conclude from both studies that the plasma-carbonization can be very fast if the plasma parameters are quite drastic. As an illustrated example, the carbonization is complete for 5 min of duration associated to $Q_{Ar}$ = 40 sccm, $P$ = 160 W. However, it has to be underlined that while fiber undergoes such a rapid transformation, the carbonic residue has no mechanical properties and breaks apart as a powder once manipulated.

For a fine-tuning of the carbonization and avoiding a too fast reaction, three different plasma-carbonization procedures based on a light experimental design were applied (Fig. 5) as follows:

- continuous plasma with discharge power or Ar flow gradient in two steps: first one an increase of power (increment each 2 min) for a plasma density rise and the second one a decrease of Ar flow (increment each 2 min) for fiber temperature rise (Fig. 5a);

| Duration | $t$ = 0 min | → | $t$ = 20 min | → | $t$ = 34 min |
|---|---|---|---|---|---|
| Power | $P$ = 32 W | → | $P$ = 320 W | → | $P$ = 320 W |
| Ar flow | $Q_{Ar}$ = 40 sccm | → | $Q_{Ar}$ = 40 sccm | → | $Q_{Ar}$ = 1 sccm |

- pulsed plasma with frequency gradient ($F$): decrease of Ar flow (increment each 2 min) at fixed power ($P$ = 32 W) and Ar flow ($Q_{Ar}$ = 40 sccm) for smoother fiber treatment (Fig. 5b):

| Duration | $t$ = 0 min | → | $t$ = 16 min |
|---|---|---|---|
| Frequency | $F$ = 1 MHz | → | $F$ = 1 Hz |

- combination of the two previous processes - pulsed and continuous plasma with frequency or flow gradient at fixed power ($P$ = 320 W) - (Fig. 5c):

| Duration | $t$ = 0 min | → | $t$ = 16 min | → | $t$ = 30 min |
|---|---|---|---|---|---|

| Frequency | $F$ = 1 MHz | → | $F$ = 1 Hz | → | continuous |
|---|---|---|---|---|---|
| Ar flow | $Q_{Ar}$ = 40 sccm | → | $Q_{Ar}$ = 40 sccm | → | $Q_{Ar}$ = 1 sccm |

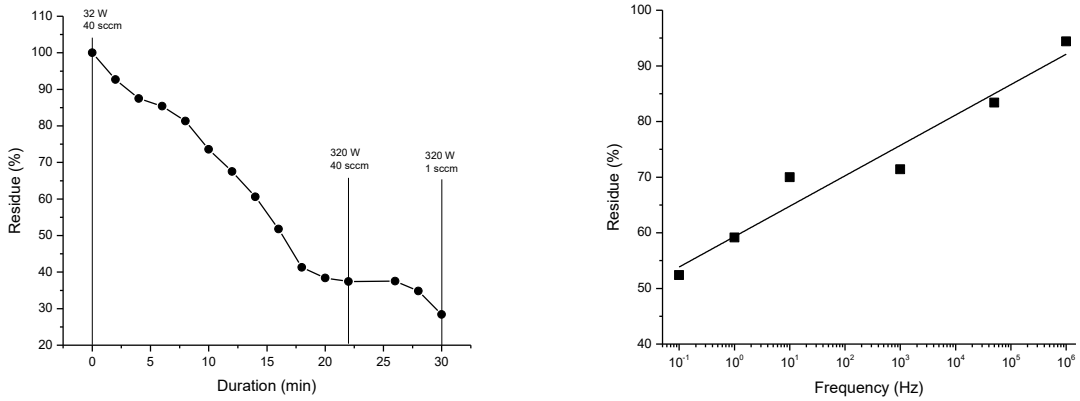


(a) (b)

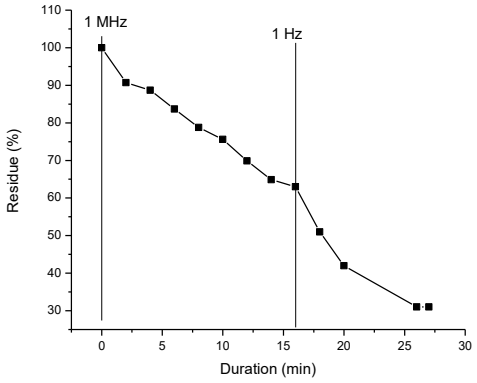


(c)

Fig. 5 Dependence of the residue yield of 0.3% CNT CANOE fibers on different plasma parameters sets (sample-holder = Fig. 2b)

Fig. 5a shows that the mass loss is proportional to discharge power and duration at fixed Ar flow, but is not altered by the flow decrease and finally the residue yield reaches a value of 28 % at 1 sccm suggesting degradation and depolymerization rather than carbonization. In pulsed plasma mode (Fig. 5b), the residue proportion varies linearly with the frequency, highest with short pulse. However, it never reaches the stoichiometric value (44.5 %) of carbonization. The combination of the both modes of plasma initiation (Fig. 5c) leads to a mass loss rate linearly dependent on pulse sequence and a minimum value of 31 % is obtained.

In conclusion of this parametric study, the residue appearance and the carbonization rate are controlled by adjusting various plasma parameters. However, this characteristic is not the only property for obtaining the true CF. Their morphological aspect, crystalline structure and mechanical behavior must be taken into account.

### *3.4. Morphological structure of the plasma-carbonized 0.3% CNT CANOE fibers*

First, the morphological aspect was followed by SEM in order to prove any dimensional variation versus the plasma conditions (Table 1).

Table 1.
SEM images of plasma-carbonized 0.3 % CNT CANOE fibers

a) Dependence on duration ($P$ = 160W, $Q_{Ar}$ = 40 sccm, sample-holder Fig. 2a) (magnification: 50 µm)

| Pristine | $t$ = 1 min | $t$ = 2.5 min | $t$ = 10 min |
|---|---|---|---|
| 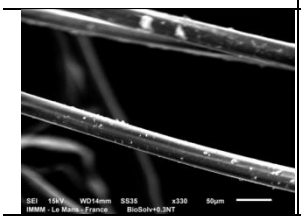 | 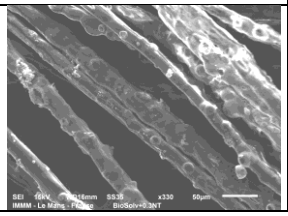 | 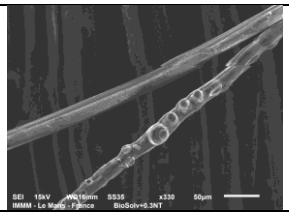 | 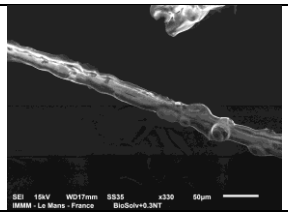 |

b) Dependence on power ($Q_{Ar}$ = 40 sccm, $t$ = 5 min, sample-holder Fig. 2a) (magnification: 50 µm)

| $P$ = 80 W | $P$ = 100 W | $P$ = 120 W | $P$ = 160 W |
|---|---|---|---|
| 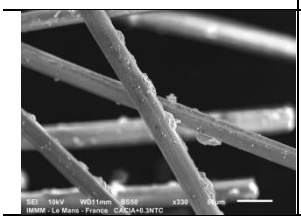 | 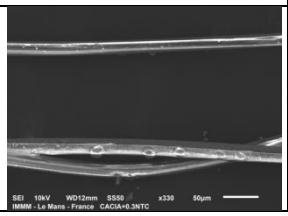 | 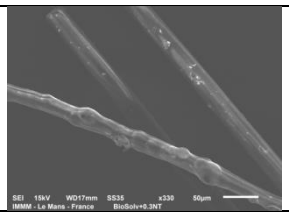 | 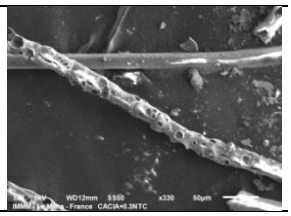 |

c) Dependence on continuous plasma with power or pressure gradient (sample-holder Fig. 2b) (magnification: 10 µm)

| | | | |
|---|---|---|---|
| Power gradient | 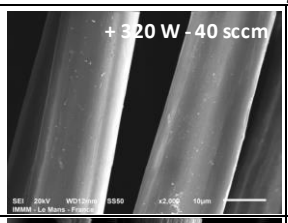 | 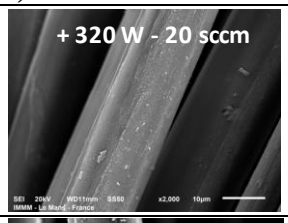 | 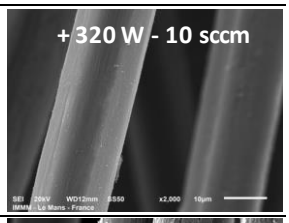 |
| Pressure gradient | 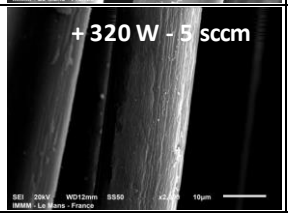 | 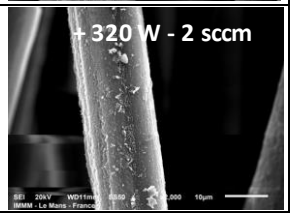 | 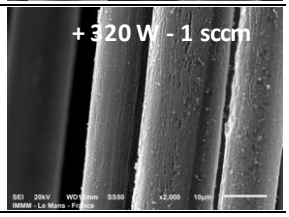 |

d) Dependence on combined pulsed and continuous plasma (sample-holder Fig. 2b) (magnification: 10 µm)

| | | | |
|---|---|---|---|
| 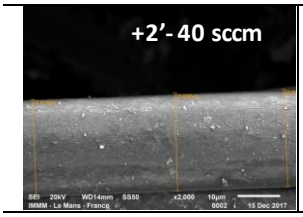 | 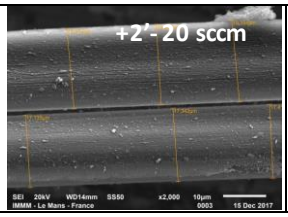 | 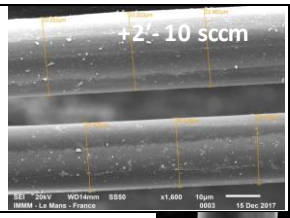 | 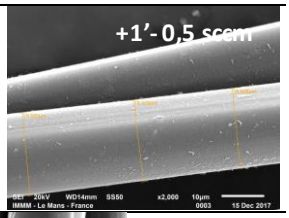 |

e) Dependence on continuous plasma - pressure monitoring (sample-holder Fig. 2b) (magnification: 10 µm)

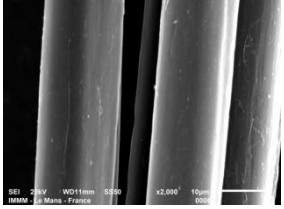

Craters are formed on the surface as early as 1 min of treatment (Table 1a). Their appearance can be assigned to the fast evaporation of degradation products during carbonization. At longer times (2 - 10 min), surface morphology remains unchanged with pinholes of 10 - 30 µm in diameter. The mean fiber diameter is decreasing from 35 µm to 22 µm at the beginning of plasma-treatment (1 min) then stabilizes for longer treatment. When varying the discharge power (Table 1b), the surface appearance of the fibers is slightly altered up to almost 120 W. Some aggregates appeared on the surface. Then, with the increase in power, the creation of pinholes, issued from degraded products' evaporation, is initiated. Their diameter and number are in relation to the power: the more important it is, the more they are formed and the larger the size they have. Thus, the carbonized fiber at 160 W seems to be porous and indeed becomes brittle. The other treatments, i.e. pulsed and/ or continuous with different gradients do not alter the surface morphology (Table 1c-e). The continuous plasma with power or pressure gradient or even their combination leads to homogeneous fibers without any porosity. A possible structure appears at argon flow equal to 5 sccm and the diameter of the fiber is decreasing from 35 µm to 17 - 20 µm. The observed small aggregates are composed of P and S impurities originating from spinning process as analyzed by EDX. Just note that the so-called pressure monitoring (Table 1e) is linked to a pressure evolution observed inside the reactor chamber when passing between different power and/or Ar flow values. It increases then after certain treatment duration, it returned to its initial level. Such an increase is significant of the appearance of volatile products generated by thermal degradation of cellulose. These variations are considered as the end of different carbonization stages after which the next step could be applied.

Raman spectroscopy allows evaluation of the degree of order of carbon atoms, i.e. to identify the appearance of graphitic planes or disordered arrangements (Byrne 2016; Faulon 1994; Kim 2015). Typically, carbon fibers have two Raman bands at 1350 $cm^{-1}$ and 1590 $cm^{-1}$, commonly known as D and G bands, respectively (Byrne 2016; Frank 2014; Paris 2005; Snowdon 2014). First band corresponds to the vibrations of the amorphous carbon while the second is assigned to the vibrations of graphitic planes. Thus, their ratio ($I_D$ / $I_G$) determines the yield of the carbon organization. Its intensity is inversely proportional to the crystallite size of the graphite that contributes to an increase in disorder. The Raman spectra (not shown here) of the different plasma-carbonized fibers present the D and G bands whose intensity is plasma parameter-dependent. The G band appears firstly. Therefore, one may conclude that the ordered graphitic structure is firstly formed under plasma treatment. In the only conditions belonging to the combined treatment, another peak assigned to the G' band at $\lambda$ = 2750 $cm^{-1}$ is observed. This band, so-called 2D band (as it is in fact the overtone of the D band) appears due to two phonons

with opposite momentum in the highest optical branch near the K point of the Brillouin zone (Ferrari 2007). Its presence indicates highly ordered graphitic structure.

The carbonization and graphitization kinetics are only studied in plasma parameters domains leading to a residue yield close to the theoretical one (44.5 %) (Fig. 6).

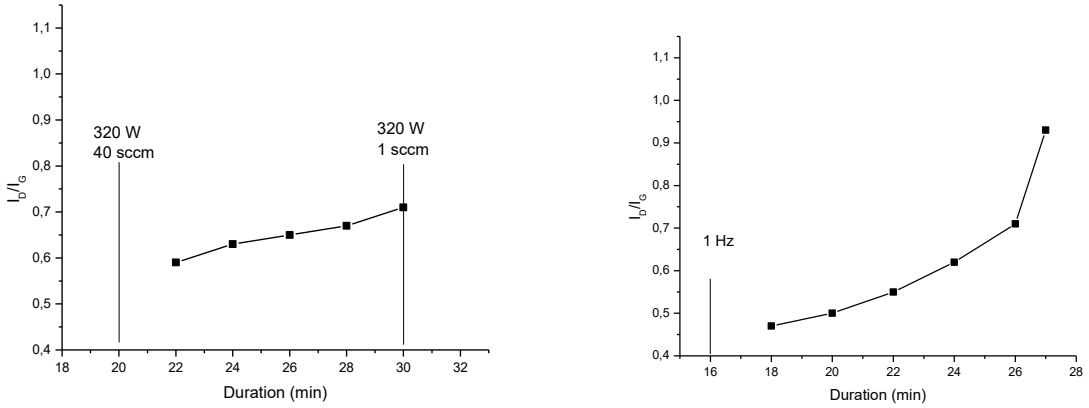


(a) (b)

Fig. 6 Dependence of the $I_D / I_G$ ratio for 0.3 % CNT CANOE fibers plasma-carbonized by (a): continuous plasma with power or pressure gradient, (b): combined pulsed and continuous plasma (sample-holder Fig. 2b)

The ratio $I_D / I_G$ is increasing during the period of increased pressure while the residue yield is almost stable around 28 %, showing a reorganization of the morphological structure of the fiber (Fig. 6a). It reaches the value of 0.7 but the reorganization must be uncompleted if compared to the obtained ratio from model ex-PAN fiber equal to 1.1. In case of combined treatment (Fig. 6b), the ratio $I_D / I_G$ is strongly and quickly increasing during the continuous phase with the pressure gradient, up to 0.95. At the end, such value is higher than that of the first experiment while both residue yields are similar (around 30 %) illustrating a further graphitic organization induced by the combined treatment. Fibers treated by pressure monitoring technique exhibit $I_D / I_G$ ratio of 1.15, matching those of ex-PAN T300. It can be concluded that this carbonization strategy yields the fibers with graphitic structure similar to ex-PAN carbon fibers.

The mechanical properties were studied thanks the measure of tensile strength of single filament samples. Whatever the applied carbonization strategy (pulsed or fixed step), all samples show similar mechanical properties, higher than untreated fibers (Table 2).

Table 2
Mechanical properties of cellulose fibers CANOE + 0.3 % CNT plasma-carbonized following different strategies (* performed by Canoe and the involved consortium)

| | Untreated | Pulsed | Continuous fixed step | Pressure monitoring | Thermal carbonization* | Ex-PAN T300 (Toray Data Sheet) |
|---|---|---|---|---|---|---|
| Tensile modulus (GPa) | 8.9 ± 0.7 | 12 ± 2 | 14.7 ± 1.5 | 25 ± 8 | 31.5 ± 2.5 | 230 |

| | | | | | | |
|---|---|---|---|---|---|---|
| Tensile strength (MPa) | 178 ± 14 | 240 ± 42 | 294 ± 30 | 449 ± 144 | 473 ± 73 | 3530 |
| Strain (%) | 1.5 ± 0.2 | 1.2 ± 0.2 | 1.3 ± 0.2 | 1.8 ± 0.3 | 1.5 ± 0.3 | 1.5 |

However, the samples carbonized with pressure monitoring seem to exhibit better mechanical strength. As one can note, measured mechanical properties are quite far from those of ex-PAN fibers and show high measurement error. This is believed to be due to material intrinsic properties and not to plasma process as obtained values are close to those for thermally carbonized fibers.

*3.5. Chemical structure of the plasma-carbonized 0.1 % CNT CANOE fibers*

The chemical structure of plasma-carbonized fibers has been characterized by FTIR (not shown here) and XPS spectroscopies. A low CNT concentration was chosen in order to obtain a better contribution of the cellulose backbone. The XPS allows identifying the chemical groups on the surface (< 10 nm) while the FTIR analyses in deeper thickness, almost in the entire fiber volume. The band at 1000 $cm^{-1}$ assigned to the C-OH bonds completely disappears suggesting scission and dehydroxylation of cellulose. This hypothesis is also supported by the disappearance of the OH band at 3000 - 3500 $cm^{-1}$. It is also noted the occurrence of a weak band at 1700 $cm^{-1}$ attributed to COOH. These results confirm the ejection of heteroatoms (essentially atomic oxygen) under the plasma bombardment in accordance with the carbonization residue curves. The XPS spectra of pristine and plasma-treated 0.1 % CNT CANOE fiber (not shown here) present mostly C1s and O1s peaks, traces of nitrogen, phosphorus, sodium, potassium, silicon and calcium were also detected. All their atomic proportions are given in the Table 3.

Table 4.

Atomic composition (XPS) of pristine or Ar plasma-treated 0.1 % CNT CANOE fiber ($Q_{Ar}$ = 40 sccm, $t$ = 5 min, $P$ = 160 W, sample-holder Fig. 2a)

| | Carbon (%at) | Oxygen (%at) | Nitrogen (%at) | O/C | Impurities (%at) |
|---|---|---|---|---|---|
| Pristine | 64 ± 3 | 35 ± 2 | $< 0.1 \pm 5\ 10^{-3}$ | 0.50 ± 0.02 | $0.1 \pm 5\ 10^{-3}$ |
| Ar plasma-treated | 91.9 ± 5.0 | 7.6 ± 0.4 | 0.30 ± 0.01 | $0.08 \pm 4\ 10^{-3}$ | $0.2 \pm 1\ 10^{-2}$ |

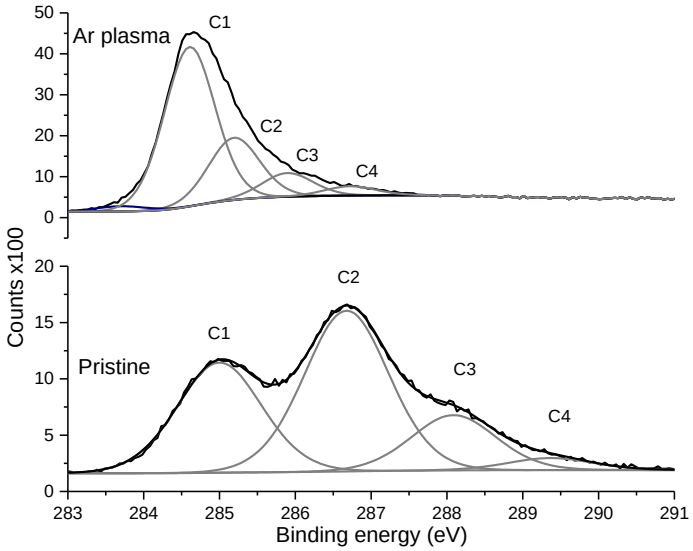


Fig. 7 High resolution C1s peak of 0.1 % CNT CANOE fibers pristine (a) and Ar plasma-carbonized (b): ($Q_{Ar}$ = 40 sccm, $t$ = 5 min, $P$ = 160 W, sample-holder Fig. 2a)

As expected, the carbon proportion of CANOE fibers treated in Ar plasma is increased up to 92 %, while the oxygen proportion dropping from 35 % to 7.6 %. This reduces the O/C ratio from 0.5 to 0.08.

The quantification of each sub-structure is given below in the Table 4.

Table 5
Decomposition and proportions of high resolution C1s peak of pristine or Ar plasma-treated 0.1 %CNT CANOE fiber ($Q_{Ar}$ = 40 sccm, $t$ = 5 min, $P$ = 160 W, sample-holder Fig. 2a)

| | Position (eV) | Assignment | Proportion (%) |
|---|---|---|---|
| Pristine | 285.0 | C-C | 32.5 |
| | 286.8 | C-C heterocycle | 47.7 |
| | 288.1 | β C-O | 16.3 |
| | 289.4 | COOR | 3.5 |
| Ar plasma-carbonized | 284.4 | graphite | 63.4 |
| | 285.2 | C-C aliph, $CH_3$ | 23.9 |
| | 285.9 | C-N, C-O, C-C heterocycle | 9.1 |
| | 286.7 | C-OH | 3.6 |

As shown in Fig. 7, the shapes of the high resolution C1s peaks of pristine or plasma-treated fibers are quite dissimilar. Indeed, the virgin sample spectrum presents broad sub-structures assigned respectively to the heterocyclic carbon centered at 286.6 eV and to the β–C-O bond at 288.1 eV. CNT structure is included in the C-C structure that also probably contains some impurities (Beamson 1992). A carboxylic structure was also detected at 289.4 eV. The high resolution C1s peak of the plasma-treated sample is narrower and the most remarkable feature is the appearance of graphite peak at 284.4 eV in the proportion of 63.4 % (Blyth 2000). The peak at 285.2 eV could be assigned to mostly hydrocarbons structure that also gives another evidence of the initiation of fiber plasma-carbonization. The other two sub-structures respectively centered at 285.9 eV and 286.7 eV are related to

the disappearance of cellulose units and the appearance of new C-O and C-N bonds, the last one probably issued from impurities included in the plasma phase or the post-oxidation.

## 4. Discussion

The plasma-carbonization mechanism should be described as originating from two types of reactions, the first one is controlled by the thermal energy, i.e. the heating of the gas while the second is initiated by the reactive plasma species. Therefore, since the fiber and its plasma interface temperatures cannot be determined, a "plasma temperature" was calculated from the plasma UV-visible emission thanks to the optical emission spectroscopy.

The recorded emission spectrum of a pure Ar plasma phase is representative of all possible electronic transitions as described in the literature ( Cullen 2015; Mohr 2005; Sarani 2010; Smith 2004; Timmermans 1999; Velmer 1974; Winchester 2004). However, the most interesting bands used for temperature calculation are situated from 400 to 455 nm. Their physical constants were retrieved from NIST database (Kramida 2018) (Table 6). The calculation details are given in experimental section.

Table 6
Optical emission bands and data used for Ar plasma temperature calculation (Kramida 2018)
1) G x A = transition probability x Einstein coefficient.

| Wavelength (nm) | Energy of upper level ($cm^{-1}$) | G x A [1)] ($s^{-1}$) | Relative intensity (a.u.) |
|---|---|---|---|
| 404.4 | 118469.0508 | 1.66e+06 | 50 |
| 415.8 | 117183.5901 | 7.00e+06 | 400 |
| 418.2 | 118459.5975 | 1.68e+06 | 50 |
| 419.1 | 116999.3259 | 1.40e+06 | 100 |
| 420.1 | 116942.7542 | 6.77e+06 | 400 |
| 425.9 | 118870.9170 | 3.98e+06 | 200 |
| 426.7 | 117183.5901 | 1.56e+06 | 100 |
| 427.2 | 117151.3264 | 2.39e+06 | 150 |
| 430.0 | 116999.3259 | 1.88e+06 | 100 |
| 433.3 | 118469.0508 | 2.84e+06 | 100 |
| 434.5 | 118407.4303 | 8.91e+05 | 25 |
| 451.0 | 117562.9553 | 1.18e+06 | 100 |

The results of this calculation are given in the Fig. 8. As expected, the excitation temperature of $Ar^{I}$ is decreasing as the flow of Ar increases and reaches a constant value at about 40 sccm (Fig. 8a). This behavior is similar to the one observed with the residue proportion. Higher Ar flow does not increase the temperature. Such a value of about 1300 °C (≈ 1573 K) is similar to the one required for the thermal carbonization. Conventional thermal process is usually conducted at 800 – 1500 °C (≈ 1073 – 1713 K), even if chemical reactions of degradation of cellulose are terminated by 400°C (≈ 673 K) ( Akato 2012; Kim 2016). The heating above this temperature is

necessary for aromatic planes to undergo rearrangement and densification to create polycyclic structure. The dependence on discharge power (Fig. 8b) is not well pronounced since the temperature is comprised between 1500 and 1600 K and should be interpreted as the fact that the plasma is initiated near the microwave applicators, then is diffusing in the overall chamber. Moreover, the optical emission is analyzed in a quite consequent volume, not specifically nearby the applicator and fiber locations. Therefore, such measure cannot discriminate on discharge power.

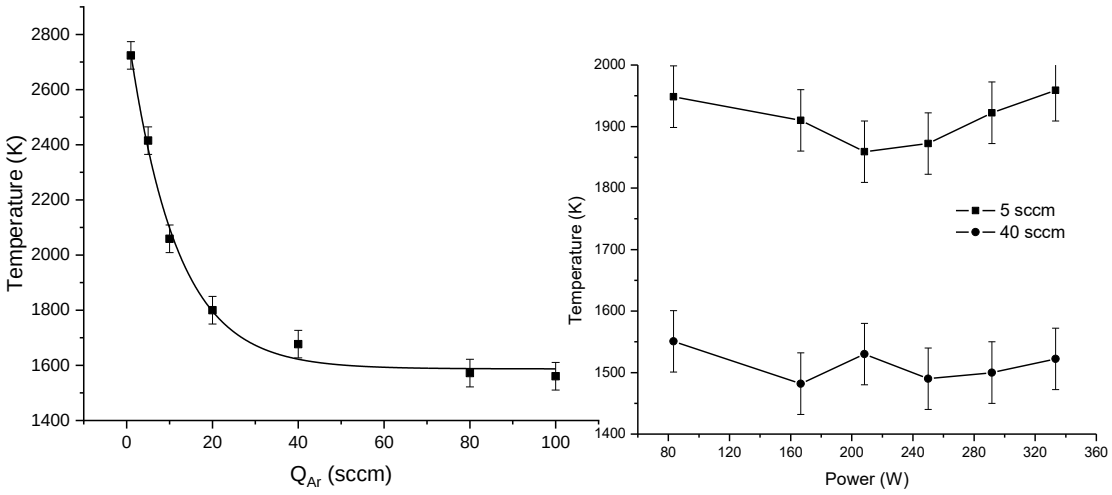


(a) (b)

Fig. 8 Dependence of the excitation temperature of $Ar^I$ in Ar plasma (a) on the Ar flow ($P$ = 320 W), (b) on the discharge power ($Q_{Ar}$ = 40 sccm)

The plasma-carbonization mechanism may be studied by tracking the evolution of the different volatile species formed during the treatment and excited in plasma phase. The comparison of emission spectra with and without fibers indicates the increase of emission intensity of a certain number of species present as traces in a pure Ar plasma (Table 6). The $H_\beta$ system ($\lambda$ = 486.6 nm) is the most intense. These bands may be related to degradation and depolymerization of the cellulose material as shown in Table 7.

As it can be seen, the presence of H and OH bands is due to the scission of lateral groups and does not imply backbone degradation. The emission of CO group can originate from both backbone depolymerization and lateral C-OH dissociation. The presence of $C_2$ emission is clearly due to main chain degradation and thus is not expected. In fact, the presence of any carbon-containing band is undesirable as it leads to the loss of carbon and the decrease of carbonization yield. In contrast, OH and H bands have to be very intense as significant of the ejection of the totality of heteroatoms. Indeed, ideal carbon fiber should not contain any defect in its structure and the presence of heteroatoms creates such defects.

Table 7
Some characteristic emission bands chosen for Ar plasma-carbonization study of 0.3 % CNT CANOE fiber ($Q_{Ar}$ = 40 sccm, $P$ = 160 W, sample-holder Fig. 2a) (Timmermans 1999) and relationship with the chemical structure of cellulose

| System | Name | λ (nm) |
|---|---|---|
| $C_2$ | Swan | 512.9 |
| | | 516.5 |
| CO | Å | 451.1 |
| | | 483,5 |
| | | 519.8 |
| | | 561.0 |
| H | Balmer | 434.5 |
| | | 486.6 |
| | | 656.5 |
| OH | - | 306.4 |

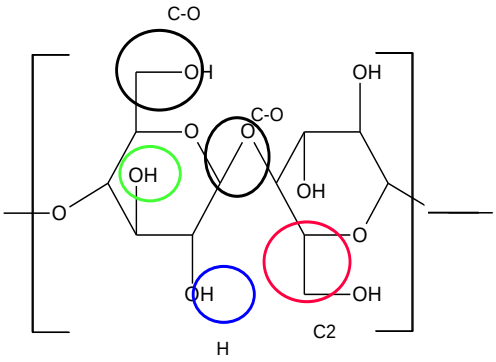


This mechanism study was followed by considering the intensity ratio of these bands in the presence (I) or not ($I_0$) of fibers. The power dependence was followed on the most intense $H_\beta$ system (λ = 486.6 nm) (Fig. 9a). Intensity ratio varies little with power up to 100 W but above this value increases rapidly showing scission on C-H and O-H bonds. Fig. 9b shows that carbonization residue is intimately linked to emission intensity of this system and therefore to the plasma chemistry, and the most significant loss of fiber mass is observed at the highest emission magnitude.

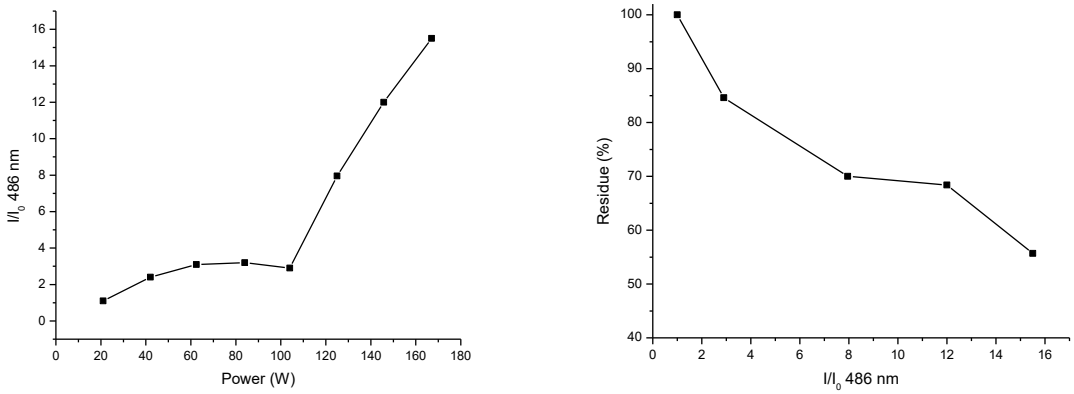


(a) (b)

Fig. 9 (a) Dependence of the ratio I / $I_0$ of $H_\beta$ intensity on discharge power for (a) plasma-carbonization study of 0.3 % CNT CANOE fiber ($Q_{Ar}$ = 40 sccm, $P$ = 160 W, sample-holder Fig. 2a) and (b) relationship between residue formation and optical emission of same Ar plasma

The kinetics of carbonization, meanwhile, was undertaken by studying the behavior of the 3 other systems less intense but more representative of the chemical functions (Fig. 10).

The bands corresponding to the C2 and CO systems undergo little evolution with the processing time, their I / $I_0$ ratio remaining close to 1. The hydroxyl band is very intense from the beginning and then decreases

exponentially to stabilize after 5 min. Its variation is similar to the one of $H_\beta$. From this study, it appears that the carbon atoms of the cellulose are not ejected during the plasma carbonization. This result confirms the result on the residue stoichiometry and that the main reaction is the scission of the OH groups followed by their dissociation partly characterized with the detection of the Balmer system. The latter should be issued from both hydrogen atoms bound to the carbon atoms but also from the dissociation of the OH groups. The shape of the different curves may suggest that hydrogen atoms bound to carbon are ejected during the first 30 s. The stabilization occurring between 30 s and 1 min is probably associated with the appearance of OH groups that may subsequently dissociate.

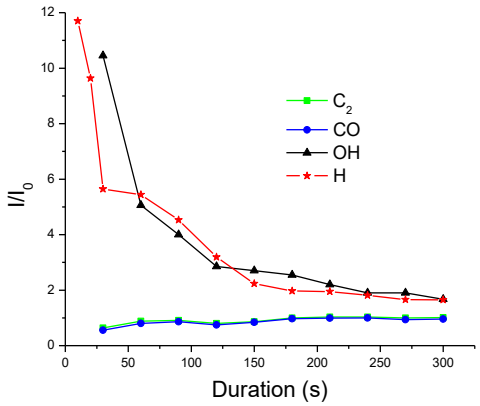


Fig. 10 Dependence of the ratio I / $I_0$ of $H_\beta$, $C_2$, CO, OH intensities on duration for Ar plasma-carbonized 0.3 % CNT CANOE fiber ($Q_{Ar}$ = 40 sccm, $P$ = 160 W, sample-holder Fig. 2a)

Another method of monitoring the advancement of carbonization is to follow the pressure variation in the plasma chamber during the process. Indeed, volatile products released during carbonization create pressure variation inside the plasma chamber. These products are not released continuously at any plasma condition, but step-wise at several specific microwave power values. It was established experimentally that for given gas flow rate (40 sccm) these values are 50 W, 83 W, 117 W and 200 W. Apparently, these values correspond to specific temperatures necessary to initiate different chemical reactions in cellulose. Proceeding at each step for duration necessary for the pressure to drop to its initial value allows for completion of respective reaction.

## 5. Conclusion

Plasma-carbonization of home-spinned cellulose fibers gives rise to a more important residue yield than during conventional thermal carbonization. Furthermore, the addition of CNT in different proportions allows the residue to be increased to the high value (30 %) at a rate of CNT ≥ 0.3 %. Raman spectroscopy shows that the carbon order is plasma parameter-dependent with increased ratio of D/G bands. Applying mechanical strain during

plasma carbonization allows obtaining non-porous fibers with smooth homogeneous surface. Mechanical properties (strain and modulus) of these fibers are higher than for pristine cellulose, but less than for ones resulting from conventional thermal carbonization. The best carbonized fiber is produced in a continuous plasma with discharge power or Ar flow gradient in two steps: first one an increase of power for a plasma density rise and the second one a decrease of Ar flow for fiber temperature rise. Its carbonization yield is close to the theoretical value, the obtained fiber is smooth, well ordered and exhibits equivalent mechanical properties as the same fiber thermal-carbonized.

Optical emission spectroscopy demonstrates that the plasma-carbonization mechanism essentially involves the ejection of hydroxyl groups from cellulose and their subsequent dissociation in plasma phase. The resulting fibers have a functionalized surface by carboxylic groups and carbon fibers with good mechanical properties have been obtained.

This paper deals with the plasma-synthesis of carbon fiber and the characterization of the obtained fiber. Therefore, we think that it fits the standard of the journal. Furthermore, we stated that:
our manuscript was not submitted to another journal
the submitted work is original and not published elsewhere
the study was not split into several parts to increase the submission number
there is no concurrent publication and results are clearly presented.

**References**


Akato K (2012) Pretreatment and pyrolysis of rayon-based precursor for carbon fibers. PhD thesis, University of Tennessee.

Beamson G, Briggs D (1992) High resolution XPS of organic polymers. New York: Wiley.

Blyth RIR, Buqa H, Netzer FP, Ramsey MG, Besenhard JO, Golob P, Winter M (2000) XPS studies of graphite electrode materials for lithium ion batteries. Appl Surf Sci 167:99-106. https://doi.org/10.1016/S0169-4332(00)00525-0

Broza G, Kwiatkowska M, Rosłaniec Z, Schulte K (2005) Processing and assessment of poly(butylene terephthalate) nanocomposites reinforced with oxidized single wall carbon nanotubes. Polymer 46:5860-5867. https://doi.org/10.1016/j.polymer.2005.05.073

Byrne N, Setty M, Blight S, Tadrov R, Ma Y, Sixta H, Hummel M (2016) Cellulose-derived carbon fibers produced via a continuous carbonization process : Investigating precursor choice and carbonization conditions. Macromol Chem Phys, 217:2517-2524. https://doi.org/10.1002/macp.201600236

Cullen PJ, Milosavljević V (2015) Spectroscopic characterization of a radio-frequency argon plasma jet discharge in ambient air. Prog Theor Exp Phys 2015(6):1-17. https://doi.org/10.1093/ptep/ptv070

Delhaes P (2013) Carbon based solids and materials. London: John Wiley & Sons, Ltd.

Dumanh AG, Windle AH (2012) Carbon fibres from cellulosic precursors: a review. J Mater Sci 47:4236-4250. https://doi.org/10.1007/s10853-011-6081-8

Faulon JL, Hatcher PG, Fadon J (1994) Is there any order in the structure of lignin? Energy & Fuels 8(2):402-407.

Ferrari AC (2007) Raman spectroscopy of graphene and graphite : Disorder , electron - phonon coupling, doping and nonadiabatic effects. Solid State Commun143:47-57. https://doi.org/10.1016/j.ssc.2007.03.052

Frank E, Hermanutz F, Buchmeiser MR. Carbon fibers: precursors, manufacturing, and properties (2012) Macromol Mater Eng, 297(6):493-501. https://doi.org/10.1002/mame.201100406

Frank E, Steudle LM, Ingildeev D, Sporl JM, Buchmeiser MR (2014) Carbon fibers: precursor systems, processing, structure, and properties. Angew Chemie - Int Ed 53(21):5262-5298. https://doi.org/10.1002/anie.201306129

Goodhew PJ, Clarke AJ, Bailey JE (1975) A review of the fabrication and properties of carbon fibres. Mater Sci Eng 17:3-30. https://doi.org/10.1016/0025-5416(75)90026-9

Kim M, Park M, Lee Y (2016) Cellulose-based carbon fibers prepared using electron-beam stabilization. Carbon Lett18:56-6. http://dx.doi.org/10.5714/CL.2016.18.056

Kim SY, Kim SY, Seong Y, Lee S, Jo S, Yeon-Ho I, Lee HS (2015) Microwave plasma carbonization for the fabrication of polyacrylonitrile-based carbon fiber. Polymer 56:590-595. https://doi.org/10.1016/j.polymer.2014.11.034

Kim SY, Kim SY, Choi J, Lee S, Jo S, Seong M, Joo J, Lee HS (2015) Two step microwave plasma carbonization including low plasma power pre-carbonization for polyacrylonitrile based carbon fiber. Polymer 69:123-128. https://doi.org/10.1016/j.polymer.2015.05.040

Konkin AA (1985) Production of cellulose based carbon fibrous materials in Strong fibres, W. Watt, B. V. Perov, Eds. Amsterdam: Elsevier Science Publishers, 275–325.

Kramida A, Ralchenko Y, Reader J, Team NA (2018) NIST Atomic Spectra Database National Institute of Standards and Technology, Gaithersburg, MD.

McNally T. et al. (2005) Polyethylene multiwalled carbon nanotube composites Polymer 46:8222-8232. https://doi.org/10.1016/j.polymer.2005.06.094

Mohr C, Vio W (2005) Investigations of an atmospheric pressure plasma jet by optical emission spectroscopy. Surf Coatings Technol 200:827-830. https://doi.org/10.1016/j.surfcoat.2005.02.217

Pappa AA, Tzamtzis NE, Statheropoulos MK, Liodakis SE, Parissakis GK (1995) A comparative study of the effects of fire retardants on the pyrolysis of cellulose and Pinus halepensis pine-needles. J Anal Appl Pyrolysis 31:85-100. https://doi.org/10.1016/0165-2370(94)00821-H

Paris O, Zollfrank C, Zickler GA (2005) Decomposition and carbonisation of wood biopolymers - a microstructural study of softwood pyrolysis. Carbon 43:53-66. https://doi.org/10.1016/j.carbon.2004.08.034

Paulauskas FL, Yarborough KD, Meek TT (2002) Carbon Fiber Manufacturing via Plasma Technology, US patent 6,372,192 B1.

Price D, Horrocks AR, Faroq AA (1997) Influence of flame retardants on the mechanism of pyrolysis of cotton (cellulose) fabrics in air. J Anal Appl Pyrolysis 40-41:511-524. https://doi.org/10.1016/S0165-2370(97)00043-0

Ramiah MV (1970) Thermogravimetric and differential thermal analysis of cellulose, hemicellulose, and lignin. J Appl Polym Sci14(5):1323-1337. https://doi.org/10.1002/app.1970.070140518

Ryan KP, Coleman JN (2007) Carbon nanotubes for reinforcement of plastics ? A case study with poly(vinyl alcohol). Compos Sci Technol 67:1640-1649. https://doi.org/10.1016/j.compscitech.2006.07.006

Sarani A, Nikiforov AY, Ley C (2010) Atmospheric pressure plasma jet in Ar and spectroscopy and temperature measurements mixtures : Optical emission Atmospheric pressure plasma jet in Ar and Ar / $H_2O$ mixtures. Phys. Plasmas17(6):063504. https://doi.org/10.1063/1.3439685

Schalamon WA, Bacon R. (1973). Process for producing carbon fibers having a high Young's modulus of elasticity. US patent 3,716,331.

Smith DJ, Whitehead CJ, Stewart R (2004) Plasma electron energy distributions measured by trace rare gases optical emission spectroscopy. J Phys D Appl Phys 37:217-236.

Snowdon MR, Mohanty AK, Misra M (2014) A study of carbonized lignin as an alternative to carbon black. ACS Sustain Chem Eng 2(5):1257-1263. https://doi.org/10.1021/sc500086v

Tang MM, Bacon R (1964) Carbonization of cellulose fibers-I Low temperature pyrolysis Carbon 2:211-220. https://doi.org/10.1016/0008-6223(64)90035-1

Timmermans EAH, Jonkers J, Rodero A, Quintero MC, Sola A (1999) The behavior of molecules in microwave-induced plasmas studied by optical emission spectroscopy. 2 : Plasmas at reduced pressure, Spectrochim. Acta - Part B At Spectrosc 54:1085–1098. https://doi.org/10.1016/S0584-8547(99)00050-6

Velmer FA, Kniseley RN (1974) Inductively coupled plasma - Optical emission spectroscopy. Anal Chem 46(13):1110-1120.

Winchester MR, Payling R (2004) Radio-frequency glow discharge spectrometry: a critical review. Spectrochim. Acta Part B At. Spectrosc 59(5):607-666. https://doi.org/10.1016/j.sab.2004.02.013

Yang H, Yan R, Chen H, Lee DH, Zheng C (2007) Characteristics of hemicellulose, cellulose and lignin pyrolysis. Fuel;86(12-13):1781-1788. https://doi.org/10.1016/j.fuel.2006.12.013